Supplement of Atmos. Chem. Phys., 24, 12323–12340, 2024
https://doi.org/10.5194/acp-24-12323-2024-supplement

Atmospheric Chemistry and Physics Open Access

Supplement of

Ozone deposition measurements over wheat fields in the North China Plain: variability and related factors of deposition flux and velocity

Xiaoyi Zhang et al.

Correspondence to: Wanyun Xu (xuwy@cma.gov.cn) and Xiaobin Xu (xiaobin_xu@189.cn)

List of Contents:

Figure S1: The satellite map of Gucheng site (Generated by ArcGIS and python code).

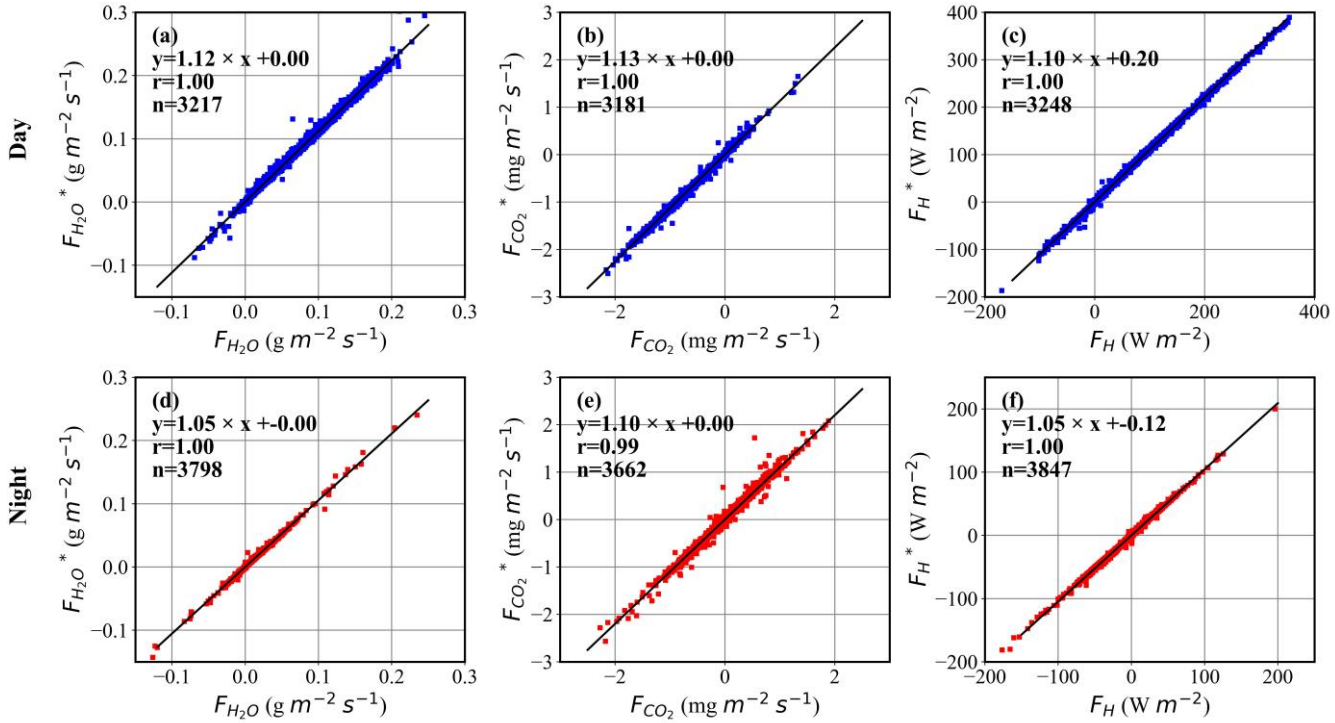

Figure S2: The influences of wind dead-bands (w_0) on REA-H_2O (a, d), REA-CO_2 (b, e) and REA-heat (c, f) fluxes in the daytime (a-c) and nighttime (d-f) from 12 February to 18 June, driven by EC raw data with a constant b = 0.60. F^* and F represent the REA fluxes with and without w_0, respectively. The linear regressions and correlation coefficients (r) between F^* and F are inset in each figure, and n is the total number of the valid fluxes.

35

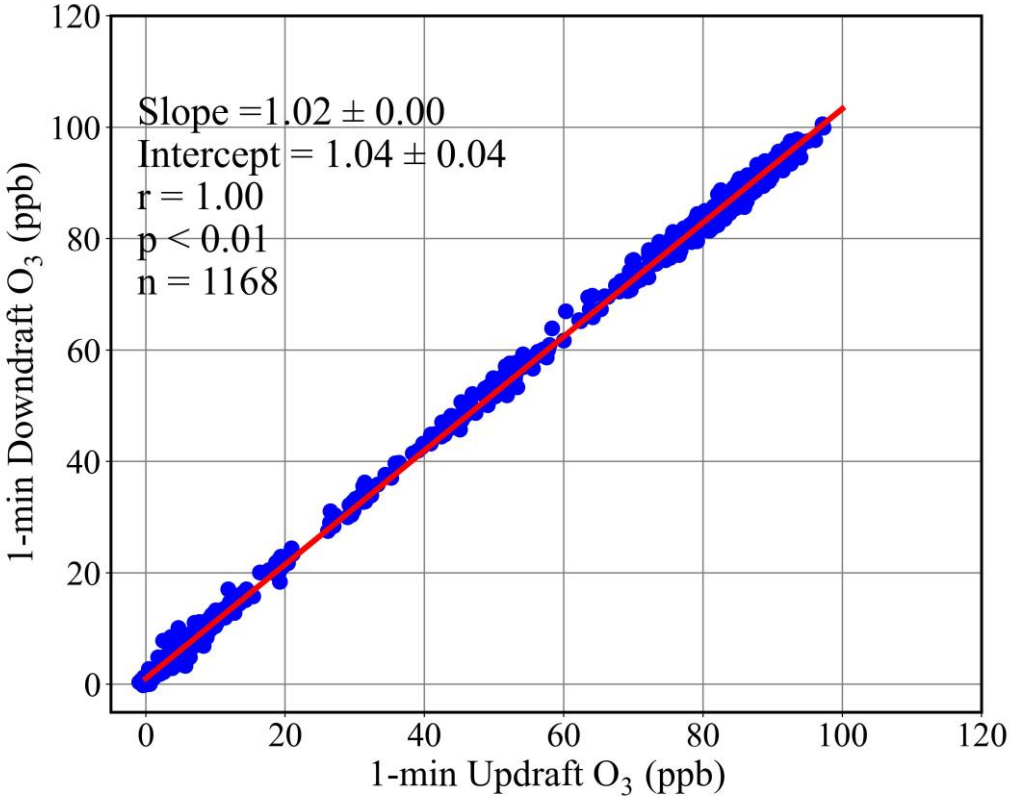

Figure S3: The comparison of O_3 concentration in the updraft and downdraft reservoirs during 10-11 May.

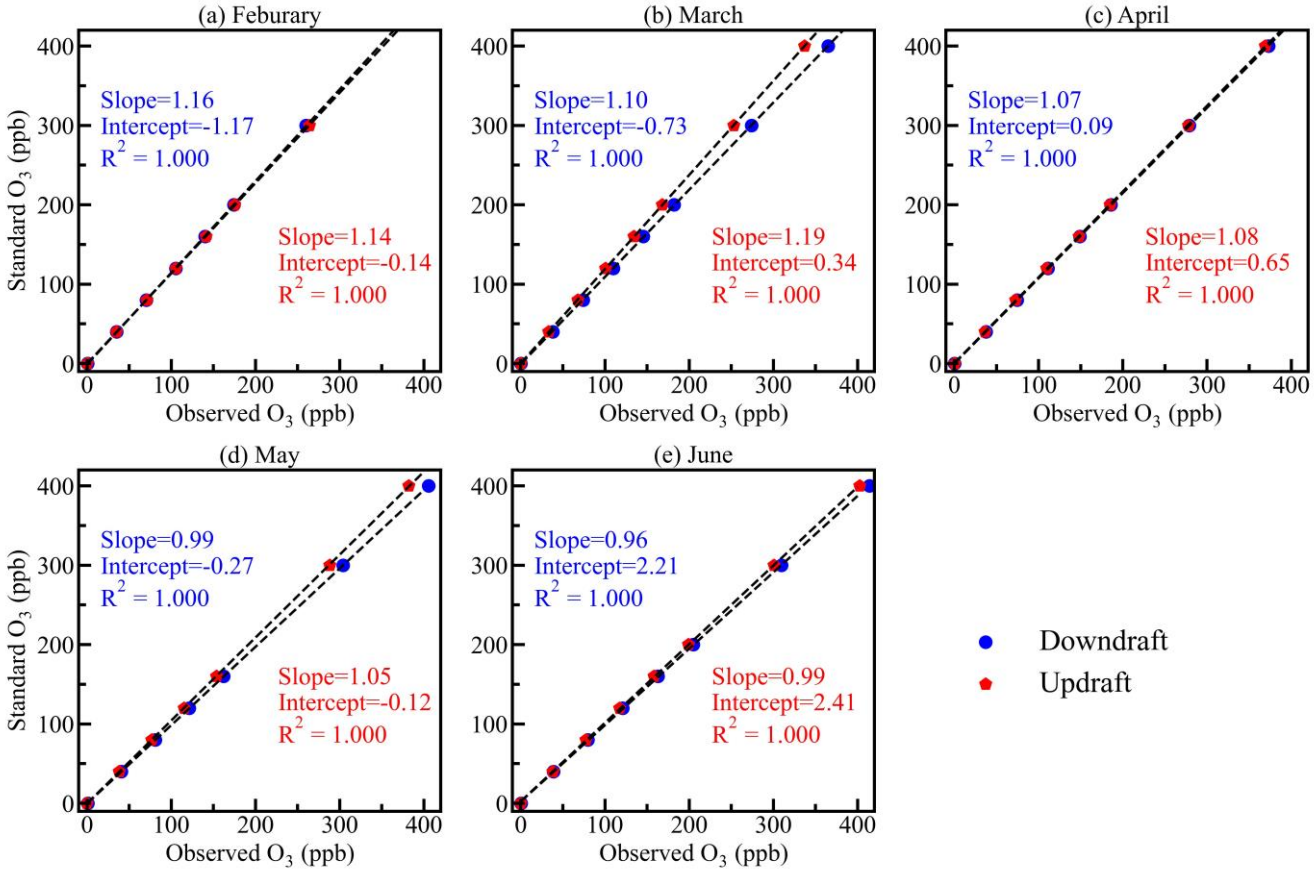

Figure S4: The results of multipoint calibration in the updraft and downdraft reservoirs.

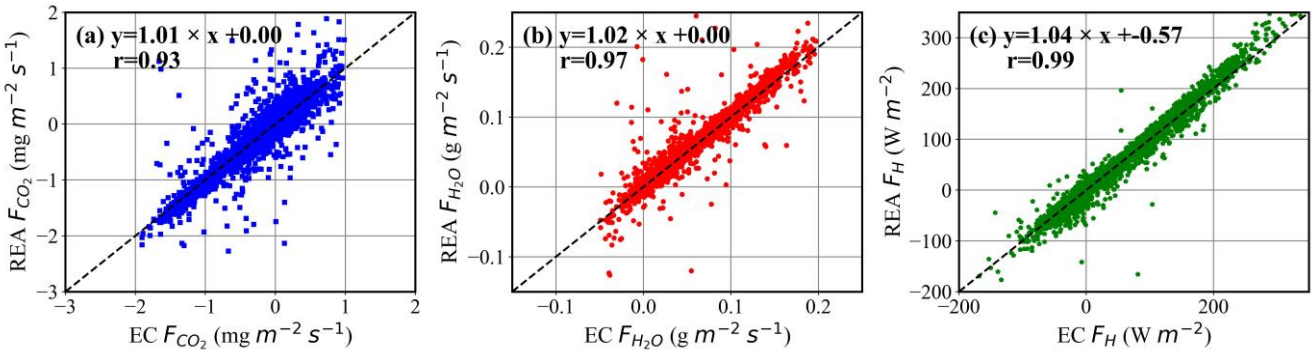

Figure S5: The comparison of CO_2 (a), H_2O (b) and heat (c) fluxes driven by EC theory and REA technique with a constant b = 0.60 and w_0. The linear regressions and correlation coefficients (r) between two fluxes are inset in each figure.

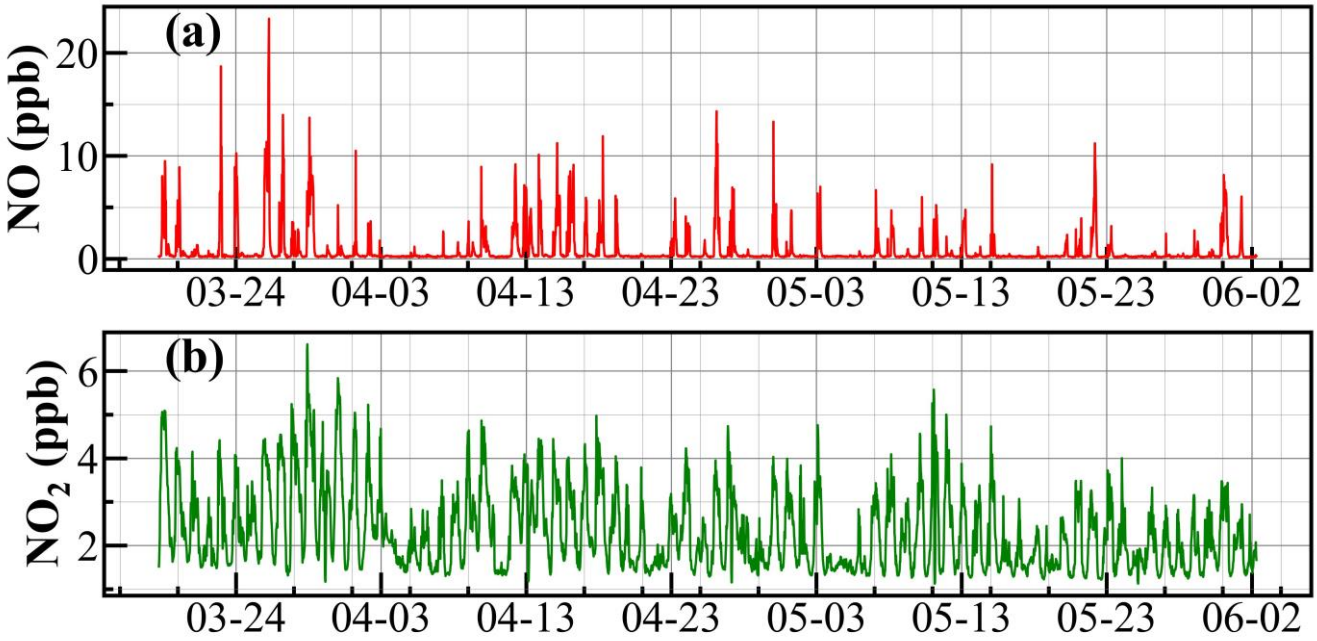

Figure S6: Timeseries of NO (a) and NO_2 (b) concentration from 18 March to 2 June.

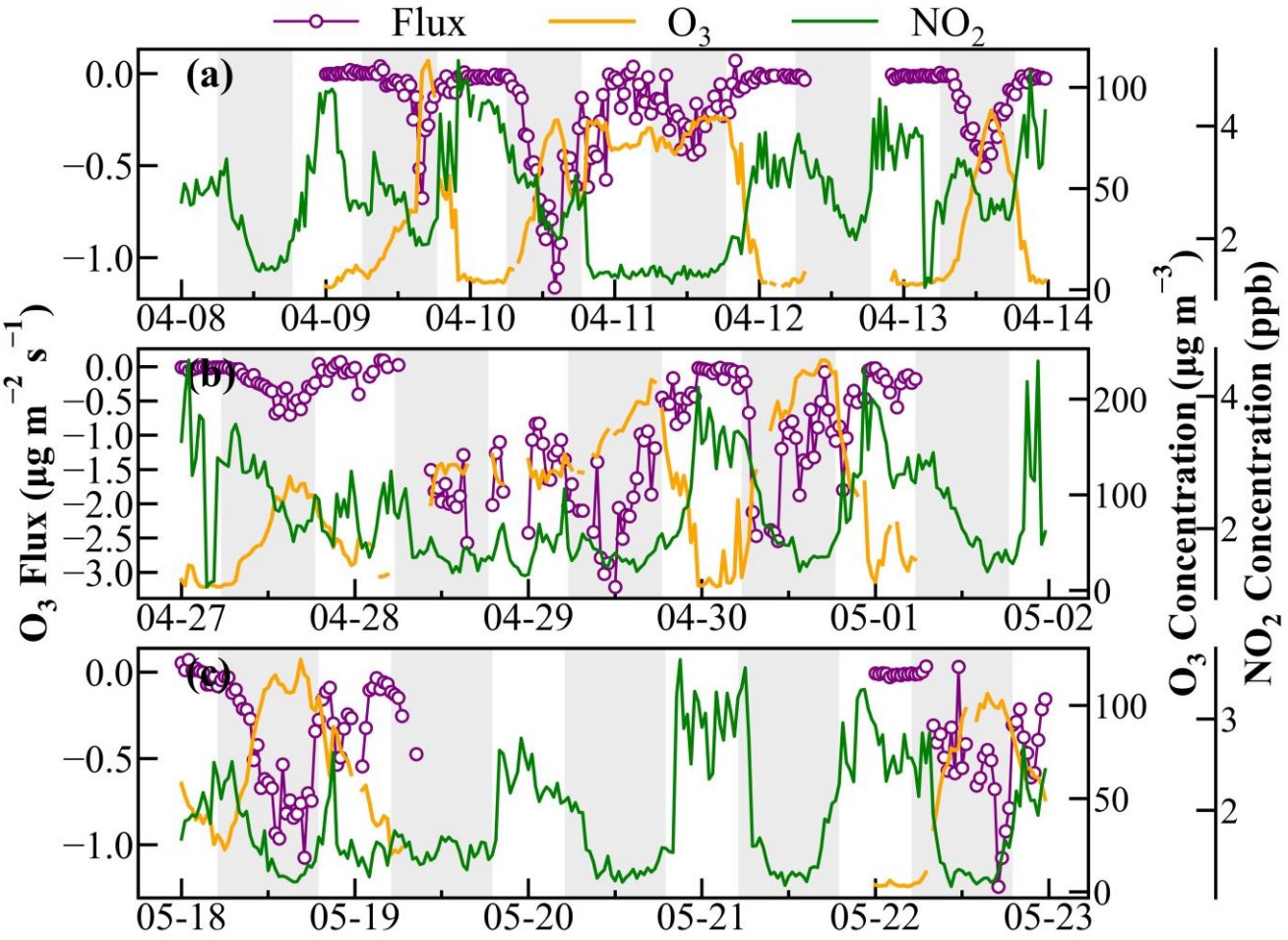

Figure S7: Variations of O_3 flux (purple lines), concentration (orange lines), NO_2 concentration (green lines) during (a) 8-13 April, (b) 27 April-1 May and (c) 18-22 May, with shades representing daytime hours.

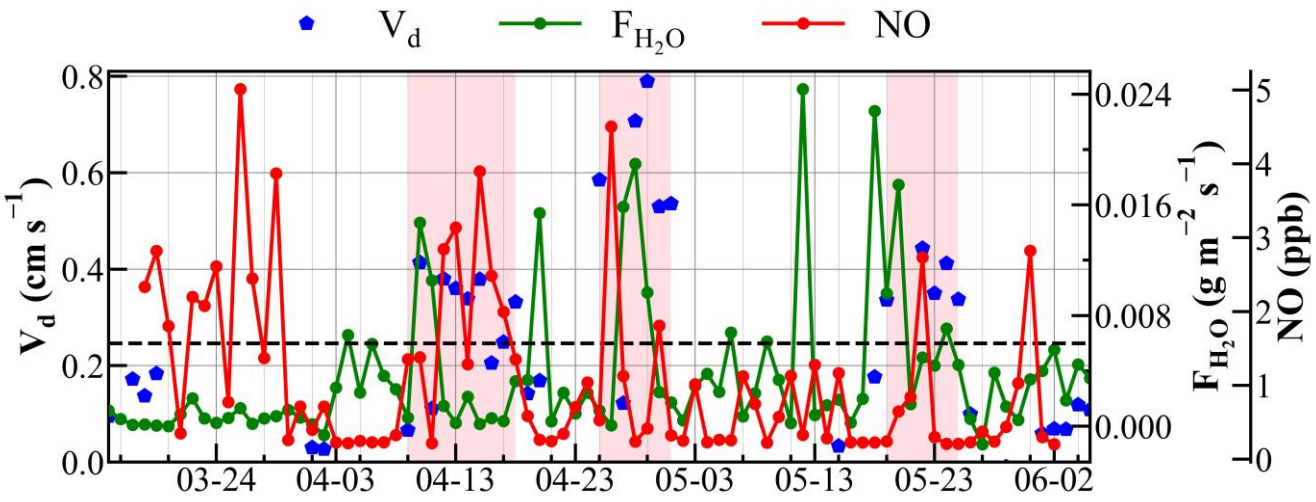

Figure S8: Variations of nighttime averaged O_3 deposition velocity (V_d, blue circle lines), H_2O flux (F_{H_2O}, green lines) and NO concentration (red lines) during 18 March-2 June.

Table S1: Winter wheat phenology at GC during 2022-2023.

Stage	Sowing	Emergence	Three-leaf	Tillering	Dormancy	Greening	Standing
Date	2022.10.18	2022.10.28	2022.11.19		2022.11.29	2023.03.02	2023.03.21
Stage	Elongation	Booting	Heading	Flowering	Milk-ripe	Ripening	Harvest
Date	2023.04.01	2023.04.15	2023.04.27	2023.05.05	2023.05.25	2023.06.11	2023.06.18

Table S2: Summary of selected O_3 deposition velocity (V_d).

Surface type	Date	Metrics	V_d (cm s^{-1})	Site	Method	References
Wheat	2016.3.16-5.30	Mean	0.39	Nanjing, China	EC	(Xu et al., 2018)
	2012.3.7-6.7	Day Mean	0.42	Yucheng, China	EC	(Zhu et al., 2015)
		Night Mean	0.14			
Maize	2011.8.9-9.28	Day mean	0.29	Yucheng, China	EC	(Zhu et al., 2014)
		Night mean	0.09			
	2002 summer	Mean	0.5	Grignon, France	EC	(Lamaud et al., 2009)
Potato	2006 summer	Mean	0.66	Scotland, England	EC	(Coyle et al., 2009)
Grassland	May 2000	Mean	0.22±0.22	Braunschweig, Germany	EC	(Mészáros et al., 2009)
	May 2001- Nov. 2004	Median	0.48±0.37	Scotland, England	FG/EC	(Coyle, 2005)
Moorland	1995-1998	Mean, at 0-40 ppb	0.75	Auchencorth Moss, Scotland	FG/EC	(Fowler et al., 2001)
	1995-1998	Mean, at 40-80 ppb	0.4			
Forest	2000-2009	Range	0.11-0.42	Hyytiälä, Finland	EC	(Rannik et al., 2012)
	1993-2000	Median	0.30	Massachusetts, America	EC	(Wu et al., 2015)
			0.35		FG [c]	
			0.35		FG [d]	
			0.62		FG [e]	
Soil	2001.4.30-5.31	Mean	0.21±0.21	La Crau, France	EC	(Stella et al., 2019)
	2008-2010 [a]		0.29±0.33	Lamasquere, France		
	2007.10.19-2008.3.4		0.26±0.20	La Cape Sud, France		
	2011.3.17-5.5		0.36±0.28	Lusignan, France		
	2014.3.24-4.14		0.61±0.48	Turro, Italy		
Sea	2006-2008	Range	0.01-0.24	Gulf of Mexico	EC	(Bariteau et al., 2010)
	2006-2008	Range	0.009-	— [b]	EC	(Helmig et al.,

	0.034	2012)

EC represents eddy covariance (EC) method, and FG refers flux-gradient (FG) approach.

[a] The specific observation periods includes 2008.4.24-5.26, 2008.11.20-12.18, 2009.11.14-2010.5.12 and 2010.9.29-11.9.

[b] The seas includes The Gulf of Mexico, Eastern Pacific Ocean, Western Atlantic Ocean and Southern Ocean.

[c] Modified micrometeorological gradient method.

[d] Modified Bowen ratio gradient method.

[e] Aerodynamic gradient method.

Table S3: The relationships of O_3 deposition velocity (V_d) and friction velocity (u_*), soil volumetric water content (soil VWC) at different ranges of LAI.

		Slope	Intercept	Std. Err.	p-value	r	n
$V_d \sim u_*$	LAI<1	0.84	0.09	0.32	0.00	0.39	158
	1≤LAI<2	1.13	0.04	0.67	0.00	0.45	48
	2≤LAI<3	2.36	0.01	0.40	0.00	0.57	282
	LAI≥3	1.91	0.15	0.49	0.00	0.42	285
$V_d \sim$ soil VWC	LAI>3.0	4.42	-1.23	1.01	0.00	0.46	285
	LAI>3.5	7.25	-2.30	2.02	0.00	0.46	186
	LAI>4.0	8.44	-2.86	2.40	0.00	0.52	132
	LAI>4.5	15.32	-5.86	5.61	0.00	0.67	39

Supplementary Method: The impact evaluation of the chemical reaction on O_3 flux measurement.

The comparison between the total residence time of the REA system and the chemical reaction time was used to evaluate to the influence of the chemical reaction on O_3 flux measurement. In the two shade channels, O_3 mainly reacted with NO, which could occur in minutes in agricultural fields (Zhang et al., 2024). In our study, since there was no simultaneous observation of the NO concentration in the two channels, we calculated the lifetime (τ_{chem}) of O_3 reacting with NO using the ambient NO concentration, and the actual τ_{chem} in the two channels would be larger than the estimated values.

$$\tau_{chem} = \frac{1}{C_{NO} \times k_r}, \quad \text{Eq. (S1)}$$

$$k_r = 0.444 \times \exp(1360/(T_{Air} + 273.15)), \quad \text{Eq. (S2)}$$

where C_{NO} is NO concentration, ppb; k_r is the reaction rate constant, $ppb^{-1}\ s^{-1}$ (Walton et al., 1997); T_{Air} is the air temperature.

From 18 March to 2 June, NO concentration ranged from 0.1 ppb to 23.3 ppb with an average of 0.8 $\pm$ 1.8 ppb. The calculated τ_{chem} of O_3 in the atmosphere ranged from 141 s to 31559 s, with an average of 8893 s, which were remarkably higher than the total residence time (~ 10 s) from tip of the inlet to the point of O_3 detection the REA system. It indicated that the chemical O_3 consumption in the two channels would be minor and might have a marginal effect on flux measurements.

References

Bariteau, L., Helmig, D., Fairall, C. W., Hare, J. E., Hueber, J., and Lang, E. K.: Determination of oceanic ozone deposition by ship-borne eddy covariance flux measurements, Atmos. Meas. Tech., 3, 441-455, 10.5194/amt-3-441-2010, 2010.

Coyle, M.: The gaseous exchange of ozone at terrestrial surfaces : non-stomatal deposition to grassland,

Coyle, M., Nemitz, E., Storeton-West, R., Fowler, D., and Cape, J. N.: Measurements of ozone deposition to a potato canopy, Agricultural and Forest Meteorology, 149, 655-666, https://doi.org/10.1016/j.agrformet.2008.10.020, 2009.

Fowler, D., Flechard, C., Cape, J. N., Storeton-West, R. L., and Coyle, M.: Measurements of Ozone Deposition to Vegetation Quantifying the Flux, the Stomatal and Non-Stomatal Components, Water, Air, and Soil Pollution, 130, 63-74, 10.1023/A:1012243317471, 2001.

Helmig, D., Lang, E. K., Bariteau, L., Boylan, P., Fairall, C. W., Ganzeveld, L., Hare, J. E., Hueber, J., and Pallandt, M.: Atmosphere-ocean ozone fluxes during the TexAQS 2006, STRATUS 2006, GOMECC 2007, GasEx 2008, and AMMA 2008 cruises, J. Geophys. Res. Atmos., 117, https://doi.org/10.1029/2011JD015955, 2012.

Lamaud, E., Loubet, B., Irvine, M., Stella, P., Personne, E., and Cellier, P.: Partitioning of ozone deposition over a developed maize crop between stomatal and non-stomatal uptakes, using eddy-covariance flux measurements and modelling, Agricultural and Forest Meteorology, 149, 1385-1396, https://doi.org/10.1016/j.agrformet.2009.03.017, 2009.

Mészáros, R., Horváth, L., Weidinger, T., Neftel, A., Nemitz, E., Dämmgen, U., Cellier, P., and Loubet, B.: Measurement and modelling ozone fluxes over a cut and fertilized grassland, Biogeosciences, 6, 1987-1999, 10.5194/bg-6-1987-2009, 2009.

Rannik, Ü., Altimir, N., Mammarella, I., Bäck, J., Rinne, J., Ruuskanen, T. M., Hari, P., Vesala, T., and Kulmala, M.: Ozone deposition into a boreal forest over a decade of observations: evaluating deposition partitioning and driving variables, Atmos. Chem. Phys., 12, 12165-12182, 10.5194/acp-12-12165-2012, 2012.

Stella, P., Loubet, B., de Berranger, C., Charrier, X., Ceschia, E., Gerosa, G., Finco, A., Lamaud, E., Serça, D., George, C., and Ciuraru, R.: Soil ozone deposition: Dependence of soil resistance to soil texture, Atmos. Environ., 199, 202-209, 10.1016/j.atmosenv.2018.11.036, 2019.

Walton, S., Gallagher, M. W., and Duyzer, J. H.: Use of a detailed model to study the exchange of NOx and O3 above and below a deciduous canopy, Atmos. Environ., 31, 2915-2931, https://doi.org/10.1016/S1352-2310(97)00126-X, 1997.

Wu, Z. Y., Zhang, L., Wang, X. M., and Munger, J. W.: A modified micrometeorological gradient method for estimating O₃ dry depositions over a forest canopy, Atmos. Chem. Phys., 15, 7487-7496, 10.5194/acp-15-7487-2015, 2015.

Xu, J., Zheng, Y., Mai, B., Zhao, H., Chu, Z., Huang, J., and Yuan, Y.: Simulating and partitioning ozone flux in winter wheat field: the Surfatm-O3 model (in Chinese), China Environmental Science 38, 455-470, 2018.

Zhang, C., Wang, J., Zhang, Y., Xu, W., Zhang, G., Miao, G., Zhou, J., Yu, H., Zhao, W., Lin, W., Kang, L., Cai, X., Zhang, H., and Ye, C.: Improving model representation of rapid ozone deposition over soil in the central Tibetan Plateau, Environmental Science: Atmospheres, 4, 252-264, 10.1039/D3EA00153A, 2024.

Zhu, Z., Sun, X., Zhao, F., and Meixner, F. X.: Ozone concentrations, flux and potential effect on yield during wheat growth in the Northwest-Shandong Plain of China, Journal of Environmental Sciences, 34, 1-9, https://doi.org/10.1016/j.jes.2014.12.022, 2015.

Zhu, Z., Sun, X., Dong, Y., Zhao, F., and Meixner, F. X.: Diurnal variation of ozone flux over corn field in Northwestern Shandong Plain of China, Science China Earth Sciences, 57, 503-511, 10.1007/s11430-013-4797-9, 2014.